PAPER

Ion-imprinted modified molecular sieves show the efficient selective adsorption of chromium(VI) from aqueous solutions†

Junwen Li[a] and Haiming Cheng [ID] *[ab]

Molecular sieve 5A was modified with (3-aminopropyl) triethoxysilane (APTES) as the support matrix, on which 4-VP was used as the ionic imprinting group. The as-prepared IIZMS-APTES was applied as the adsorbent for the recovery of chromium(VI) from aqueous solutions. The adsorbent was characterized *via* Fourier transform infrared spectroscopy (FT-IR), scanning electronic microscopy (SEM), and X-ray diffraction (XRD). The influences of adsorption time, concentration of the ions, initial pH, and temperature on the adsorption performance to Cr(VI) were investigated. The selectivity and reusability of IIZMS-APTES are also evaluated. The results showed that the maximum adsorption capacity reached 56.46 mg g^{-1} when the initial concentration of metal ions was at 100 mg L^{-1} at pH 2 and 30 °C. The adsorption process followed the pseudo-second-order kinetic model and Langmuir adsorption isotherm model. The IIZMS-APTES exhibits an efficient selective adsorption of Cr(VI) from aqueous solutions.

1. Introduction

Industrial activities have produced a large amount of industrial wastewater, which has caused serious harm to the environment and human body. Chromium ions, both Cr(III) and Cr(VI), are considered to be typical toxic contaminants, which widely exist in industries such as electroplating, leather tanning, textile, lumbering, metal finishing processes, and pigments.[1] It has been well known that Cr(VI) is an effective mutagen and potential carcinogen, and its toxicity is 500 times more than that of Cr(III).[2,3] According to the United States Environmental Protection Agency, the maximum contaminant limits of total chromium in drinking water are less than 100 μg L^{-1}.[4] Methods have been developed for the removal of Cr(VI) from wastewater, including bio-electrochemical, chemical precipitation, membrane separation, electrolysis, and adsorption.[5–9] Among them, adsorption has been studied widely due to its easy operation, low cost, good reusability and excellent recovery efficiency. Traditional adsorbents include bio-adsorbents, magnetic nanocomposites, activated carbons, and chelating resin.[10–13] However, these adsorbents have shortcomings such as sensitive to pH, low specific surface area, poor adsorption capacity, and low selectivity. Metal organic frameworks (MOFs)

have attracted extensive attention as adsorbents for the removal of toxic metal ions due to their advantages such as large pore volume, superior adsorption capacity and easy modification.[14–16] However, MOFs have some limitations, including difficulty in mass production, poor stability in water, high cost, and insufficient adsorption selectivity. Therefore, it is highly urgent to develop adsorbents with excellent regeneration property and efficient selectivity towards Cr(VI). In 1972, Wulff *et al.*[17] proposed molecule imprinting polymers, which have been shown to be an effective way to remove heavy metal ions from industrial wastewater with good selectivity.[18–20] Furthermore, the surface ion imprinting polymer technology (IIP) was studied because the traditional IIP have innate limitations such as heterogeneous distribution of the binding sites, incomplete template removal, and slow mass transfer for the target ions. Until now, numerous IIP studies have focused on Cr(VI) adsorption. Taghizadeh[21] prepared Cr(VI)-IIP on the surface of magnetic multiwall carbon nanotubes through precipitation polymerization using 4-vinylpyridine (4-VP). Huang[22] studied a novel Cr(VI)-IIP using the surface ion imprinting technique on graphene oxide-mesoporous silica nanosheets with 3-(2-amino ethyl amino)propyl trimethoxysilane as the functional monomer and the material showed good selectivity towards Cr(VI). Neolaka[23] reported that Cr(VI)-IIP supported on the natural zeolite structure for the Cr(VI) removal from aqueous solutions, achieving the highly selective removal of Cr(VI) from low-concentration wastewater.

Zeolite molecular sieve 5A is a type of calcium ion exchange and synthetic bubble-zeolite, which possesses a larger specific surface area and more uniform aperture compared to a natural zeolite.[24–27] It is often used as a gas adsorbent and catalyst

[a]The Key Laboratory of Leather Chemistry and Engineering of Ministry of Education, Sichuan University, Chengdu 610065, China

[b]National Engineering Laboratory for Clean Technology of Leather Manufacture, Sichuan University, Chengdu 610065, Sichuan, China. E-mail: chenghaiming@scu.edu.cn

support. (3-Aminopropyl)triethoxysilane (APTES) is a silane coupling agent with amino groups, which has been showing a good capacity towards the adsorption of Cr(VI) ions.[28–30] Herein, to recover Cr(VI) ions from aqueous solutions, the APTES-modified zeolite molecular sieve 5A (ZMS-APTES) was prepared as the carrier, on which 4-VP was used as the ionic imprinting group. The adsorption study focused on the effect of operation parameters including pH, contact time, concentration of metal ions, and adsorption temperature. Adsorption kinetics, equilibrium and thermodynamic were evaluated as well. Moreover, the competing adsorption of the adsorbent towards Cr(VI), Cr(III), Zn(II), and Cu(II) were investigated.

2. Experimental

2.1 Reagents and materials

Zeolite molecular sieves 5A (ZMS-5A) and potassium dichromate ($K_2Cr_2O_7$) were purchased from Kelong Chemicals (Chengdu, China). 4-Vinylpyridine (4-VP), (3-aminopropyl)triethoxysilane (APTES), ethylene glycol dimethacrylate (EGDMA), and 2,2′-azobisisobutyronitrile (AIBN) were purchased from Aladdin (Shanghai, China). All other reagents were of analytical grade and used as received without further purification. The stock solution of Cr(VI) (1000 mg L^{-1}) was prepared by dissolving an appropriate amount of $K_2Cr_2O_7$ in deionized water (18.2 MΩ).

2.2 Modification of the molecular sieve 5A

The APTES-modified zeolite molecular sieve 5A (ZMS-APTES) was prepared according to the reported with some modifications.[31] Briefly, 2.0 g of ZMS-5A was suspended in 50 mL of methylbenzene, followed by the dropwise addition of 8 mL of APTES into the mixture. The mixture was refluxed under magnetic stirring at 110 °C for 24 h in N$_2$ atmosphere. After that, the suspended solids were filtered out and thoroughly washed with ethanol.

2.3 Synthesis of IIZMS-APTES and NIZMS-APTES

The surface ion imprinting on ZMS-APTES was synthesized through radical-induced polymerization in combination with an *in situ* co-precipitation method. Step 1: 1.0 mmol of $K_2Cr_2O_7$ and 8 mmol of 4-VP were dissolved in 60 mL of ethanol/acetone (2 : 1, v/v) in a 150 mL of flask by stirring at room temperature for 30 min to form the Cr(VI) and 4-VP complex. Step 2 (imprinting): 2.0 g of ZMS-APTES and 2.0 mL of ethylene glycol dimethacrylate (EGDMA) were added into the flask. To start the reaction, 0.1 g of AIBN was added, and then the mixture was stirred at 70 °C for 24 h in a N$_2$ atmosphere to form Cr(VI) ion imprinted polymers onto ZMS-ATPES. Step 3 (elution): after cooling to room temperature, the suspended solids were filtered out and then thoroughly washed with ethanol. 4.0 mol per L of HNO$_3$ was used for eluting the imprinted Cr(VI) ions. Further, the solids were desiccated at 65 °C to constant weight and designed as IIZMS-APTES. As a control, a non-imprinted adsorbent was prepared as the above mentioned steps, except

no $K_2Cr_2O_7$ in step 1 and without elution, which was designed as NIZMS-APTES.

2.4 Characterization

FT-IR spectra were recorded by a Nicolet Is10 Fourier transform infrared spectrometer (FT-IR) (Thermo Fisher Scientific, USA) by the KBr pellet method in the range of 4000–400 cm^{-1} with 2 cm^{-1} of resolution. Surface morphology was observed using a JSM 7500F scanning electron microscopy (SEM) (JEOL, Japan). The elemental compositions of the samples were measured *via* 51-XMX0019 X-Max energy-dispersive X-ray spectroscopy (EDXS) (Oxford Instruments, UK).

2.5 Batch adsorption experiments

The batch experiments of the IIZMS-APTES adsorption of Cr(VI) ions were investigated in a series of 50 mL polyethylene tubes. Briefly, 30 mg of the as-prepared adsorbent and 30 mL solution of varying concentrations of Cr(VI) (20–1000 mg L^{-1}) were added into the tube. The pH (1–9) of Cr(VI) solutions, the contact time (5–300 min), and the temperature (30–50 °C) were investigated. The pH of the solution was adjusted to a desired value by 0.1 mol L^{-1} of HCl or NaOH. After adsorption, the adsorbents were spinned down, and the concentration of Cr(VI) ions in the supernatant was measured *via* inductively coupled plasma-optical emission spectrometry (ICP-OES, Agilent, USA). The adsorption capacity q_e (mg g^{-1}) was calculated by eqn (1):

$$q_e = \frac{(C_0 - C_e) \times V}{m} \quad (1)$$

where C_0 (mg L^{-1}) and C_e (mg L^{-1}) are the initial and equilibrium concentrations of the metal ions, respectively; V (L) is the volume of the testing solution and m (g) is the weight of the adsorbent. All the adsorption experiments were repeated three times.

2.6 Competing adsorption

To evaluate the adsorption selectivity of IIZMS-APTES towards Cr(VI) with coexisting ions, the competitive adsorptions of Cr(VI)/Cr(III), Cr(VI)/Cu(II), and Cr(VI)/Zn(II) were investigated, respectively. 30 mg of the adsorbent with 30 mL of the solution containing 100 mg L^{-1} of each kind of metal ions was stirred at pH 3 and 30 °C for 60 min. After adsorption, the concentration of metal ions in the supernatant was determined by ICP-OES. The distribution ratio (K_d, L g^{-1}), the selectivity coefficient K and the relative selectivity coefficient K' were calculated by eqn (2)–(4):

$$K_d = \frac{(C_0 - C_e)}{C_e} \times \frac{V}{m} \quad (2)$$

$$K_{Cr(VI)/M} = \frac{K_{d(Cr(VI))}}{K_{d(M)}} \quad (3)$$

$$K' = \frac{K_{IIZMS-APTES}}{K_{NIZMS-APTES}} \quad (4)$$

Herein, the concentration of Cr(vi) in the Cr(vi)/Cr(iii) solution was determined using a diphenylcarbazide spectrophotometry assay.[32]

3. Results and discussion

3.1 Characteristic

The FT-IR spectrum of zeolite molecular sieve 5A (ZMS-5A) showed peaks at 3442 cm^{-1}, 1656 cm^{-1}, 1477 cm^{-1}, 1008 cm^{-1}, and 673 cm^{-1}, among which 3442 cm^{-1}, 1656 cm^{-1}, and 1477 cm^{-1} are the stretching vibrations and the bending vibrations of the hydroxyl group, while 1008 cm^{-1} and 673 cm^{-1} are the stretching vibrations of Si–O–Si[33] (Fig. 1a). In comparison with ZMS-5A, the vibration of N–H (2854 cm^{-1}) is observed, suggesting the successful graft of APTES onto ZMS-5A (Fig. 1b). The peak at 1727 cm^{-1} of the C=O stretching vibration could be assigned to the crosslinking agent EGDMA[18] (Fig. 1c and d). The peak at 1410 cm^{-1} is assigned to C–N of the pyridine group[34] (Fig. 1c and d); furthermore, the peaks at 1600 cm^{-1} and 1560 cm^{-1} are assigned to the aromatic ring of 4-VP, which weakened after binding with Cr(vi) anions (Fig. 1e). The results illustrate that IIZMS-APTES have been successfully prepared.

The XRD patterns of the samples are shown in Fig. 2. The characteristic peaks of ZMS-5A are in good agreement with the reported data.[35,36] The modification by APTES did not change the crystal structure of ZMS-5A. However, most of the sharp
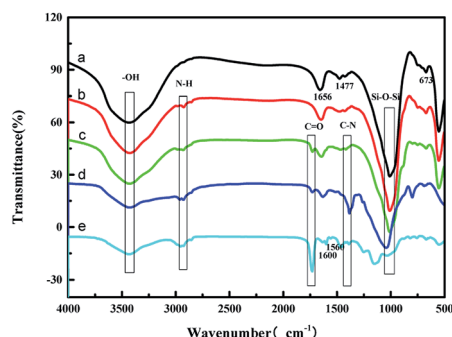

Fig. 1 FT-IR spectra of (a) ZMS-5A, (b) ZMS-APTES, (c) IIZMS-APTES before leaching, (d) IIZMS-APTES, and (e) NIZMS-APTES.
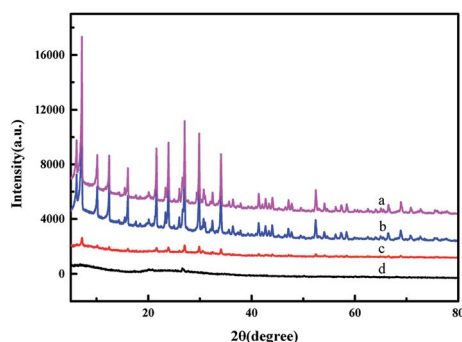

Fig. 2 The XRD spectra of (a) ZMS-5A, (b) ZMS-APTES, (c) IIZMS-APTES before leaching, and (d) IIZMS-APTES.
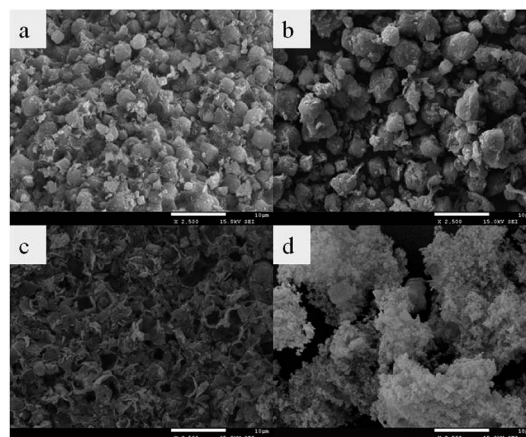

Fig. 3 The SEM images of (a) ZMS-5A, (b) ZMS-APTES, (c) IIZMS-APTES, and (d) NIZMS-APTES.

characteristic diffraction peaks of IIZMS-APTES disappeared. The formed ion imprinted polymers are coated onto the surface, which may lead the change of the crystal structure of ZMS-5A (Fig. 3c). The crystal structure of IIZMS-APTES is changed (Fig. 3d), and this may be due to the alum and silicon in the frameworks could be leached out by acid or alkaline solution during the leaching process.[37]

The typical TEM morphology of ZMS-5A is a cubic structure with rounded-off corners.[38,39] When grafted with APTES, the shape of ZMS-5A became larger and more irregular (Fig. 3b). The morphology of IIZMS-APTES was irregular and rough, which might be due to the ion imprinted polymers onto the surface (Fig. 3c). In comparison with IIZMS-APTES, the morphology of NIZMS-APTES was cloudy, which may be due to the polymer particles that are adhered onto the surface of ZMS-APTES.

The EDS analysis shows the composition of IIZMS-APTES before and after elution (Fig. 4). It can be seen that the main
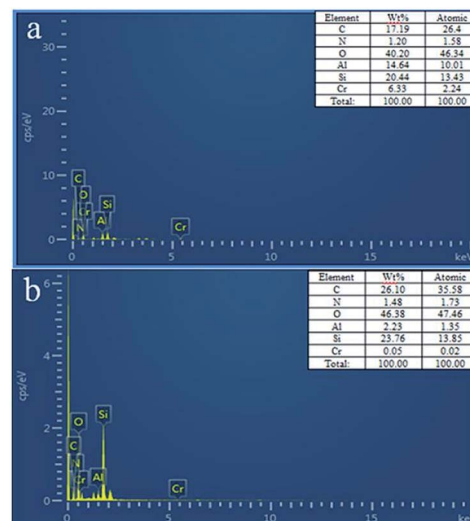

Fig. 4 The EDS images of (a) IIZMS-APTES before leaching, (b) IIZMS-APTES.

elements of IIZMS-APTES were C, N, Si, O, Al and Cr (6.33% wt) (Fig. 4a). Only a few Cr (0.05% wt) remained on IIZMS-APTES after elution (Fig. 4b). The results suggest that over 99% of Cr(VI) was eluted by 4.0 mol L^{-1} of HNO$_3$.

3.2 Cr(VI) adsorption performance

3.2.1 Effect of the initial pH. The effects of the initial pH on IIZMS-APTES adsorbing of Cr(VI) ions were performed in 50 mL polyethylene tubes containing 30 mL of 100 mg L^{-1} metal ion solutions with 30 mg of adsorbent at 30 °C for 60 min by varying the initial pH of the solution from 1.0 to 9.0 (Fig. 5a). The adsorption capacity of Cr(VI) increased with an increase in the solution pH from 1.0 to 2.0, and then decreased when the solution pH further enhanced from 3.0 to 9.0. It can be seen that the maximum adsorption capacity of Cr(VI) for both IIZMS-APTES and NIZMS-APTES was acquired at pH 2. The main reason is that Cr(VI) exists in different stable forms in aqueous solutions and the forms are dependent on pH of the solution.[40] It is known that H$_2$Cr$_2$O$_7$ exists in the solution from pH 1–2, HCrO$_4^{-1}$ and Cr$_2$O$_7^{2-}$ are in pH 2–6.5, and CrO$_4^{2-}$ is in pH value above 6.5.[41] Moreover, the surface of IIZMS-APTES has more positive charges and is more likely combine with Cr(VI) anions due to the combination of nitrogen in polymer and protons in aqueous solutions with lower pH. When the solution pH increased higher than 2, the adsorption capacity decreased and this is attributed to the amount of protonated nitrogen decreased. In pH 1–2, the reason for the low adsorption capacity is attributed to that H$_2$Cr$_2$O$_7$ cannot be combined with protonated nitrogen of the polymer matrix by electrostatic interactions.

3.2.2 Effect of the contact time. The effect of the contact time on IIZMS-APTES adsorbing of Cr(VI) ions was investigated by varying the contact time from 10 to 300 min. All experiments were performed at pH 2 and 30 °C with 30 mg of adsorbent. The results are shown in Fig. 5b. It showed that the adsorption rate was very fast in the first 30 min, and then it slowed down slightly, and reached equilibrium within 60 min. The high adsorption capacity was due to the imprinted groups had high binding ability towards Cr(VI) ions. It also can be seen that the adsorption amount of IIZMS-APTES was higher than that of NIZMS-APTES, revealing that IIZMS-APTES had a stronger affinity towards Cr(VI) than NIZMS-APTES.

In order to further investigate the adsorption kinetics, two common kinetic models,[42,43] the pseudo-first order and the pseudo-second order kinetic models, are adopted to fit the experimental data. The fitting curves are shown in Fig. S1† and
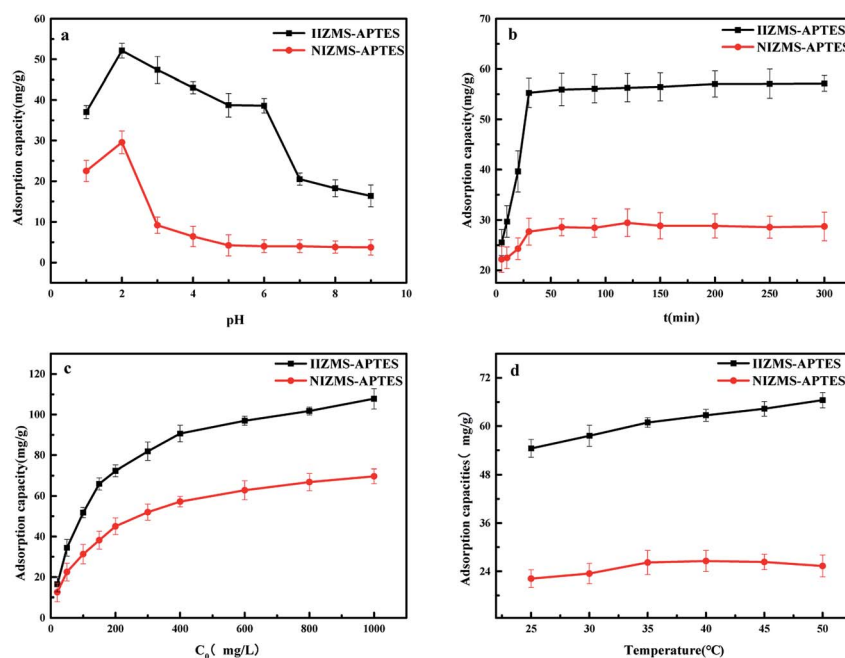

Fig. 5 Cr(VI) adsorption by IIZMS–APTES. (a) Initial pH, (b) contact time, (c) initial concentration of Cr(VI), and (d) temperature.

Table 1 Kinetic parameters for Cr(VI) adsorption by IIZMS–APTES and NIZMS–APTES

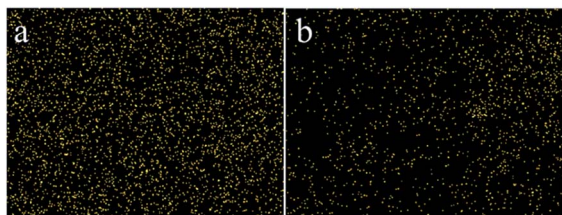| Sample	Pseudo-first-order			Pseudo-second-order		
	q_e (mg g^{-1})	k_1 (min^{-1})	R^2	q_e (mg g^{-1})	k_2 (mg g^{-1} min^{-1})	R^2
IIZMS-APTES	59.30	1.03×10^{-1}	0.8732	66.09	1.50×10^{-3}	0.9736
NIZMS-APTES	12.51	8.16×10^{-2}	0.7519	29.87	1.14×10^{-2}	0.9967

Fig. 6 The EDX maps of the Cr content on the adsorbents after adsorption. (a) IIZMS-APTES, and (b) NIZMS-APTES.

Table 3 Thermodynamic parameters of IIZMS-APTES

T (K)	q_e (mg g^{-1})	ΔG° (kJ mol^{-1})	ΔH° (kJ mol^{-1})	ΔS° (kJ K^{-1} mol^{-1})
298	54.47	−0.794	16.49	0.058
303	57.62	−1.084		
308	60.9	−1.374		
313	62.69	−1.664		
318	64.31	−1.954		
323	66.46	−2.244		

the kinetic parameters are listed in Table 1. The adsorption of Cr(VI) on IIZMS-APTES fitted well with the pseudo-second-order model, with the correlation coefficient R^2 of 0.9736. The results revealed that the adsorption of Cr(VI) on IIZMS-APTES is mainly a chemical adsorption process.

3.2.3 Effect of initial concentration. The effect of the initial concentration of Cr(VI) was investigated by varying the concentration from 20 to 1000 mg L^{-1}. All experiments were performed at pH 2 and 30 °C for 60 min with 30 mg of adsorbent. The adsorption capacity increased fast with the enhancement of concentrations of Cr(VI), and it enhanced slowly when the concentration reached 400 mg L^{-1} (Fig. 5c). It is worth noting that the adsorption capacity of IIZMS-APTES was much higher than that of NIZMS-APTES, indicating that IIZMS-APTES had more adsorption sites. The EDS map showed the distribution of Cr(VI) ions after adsorption on IIZMS-APTES and NIZMS-APTES, respectively (Fig. 6). It can be seen that the Cr(VI) ions attached on IIZMS-APTES were denser and more even than that attached on NIZMS-APTES. To confirm the adsorption properties of the system, the adsorption isotherms were evaluated with Langmuir and Freundlich models.[44,45] The fitting results are shown in Fig. S2† and Table 2. It shows that the experimental data of both adsorbents are fitted well with the Langmuir isotherm model, with the correlation coefficient (R^2) at 0.9950 (IIZMS-APTES) and 0.9937 (INZMS-APTES), respectively, indicating a monolayer uniform adsorption mode for IIZMS-APTES adsorbing Cr(VI).[45] The maximum Cr(VI) adsorption capacity (q_m) calculated by the Langmuir isotherm function was 110.62 mg g^{-1} (IIZMS-APTES) and 74.35 mg g^{-1} (NIZMS-APTES), respectively. The results illustrate that the ion imprinting process can significantly increase the adsorption capacity to Cr(VI) for IIZMS-APTES.

3.2.4 Effect of temperature. The effect of temperature for the adsorption of Cr(VI) onto IIZMS-APTES was investigated by varying the temperature at 25 °C, 30 °C, 35 °C, 40 °C, 45 °C, and 50 °C, respectively. All experiments were performed in 30 mL of
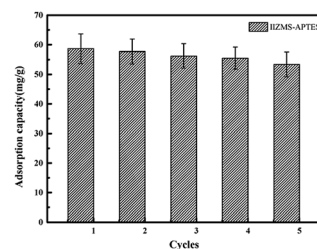

Fig. 7 Adsorption capacity of IIZMS-APTES after 5 cycles of adsorption and desorption process.

100 mg L^{-1} metal ion solutions with 30 mg of adsorbent at pH 2 for 60 min. As shown in Fig. 5d, the adsorption capacity of Cr(VI) for IIZMS-APTES was increased with an increase in the temperature in the range from 25 °C to 50 °C. However, there was no significant change of Cr(VI) adsorption on NIZMS-APTES. To further study the thermodynamic behaviour of IIZMS-APTES, the values of standard free energy (ΔG°), standard enthalpy (ΔH°), and standard entropy (ΔS°) were calculated using the van't Hoff equation[46] (Fig. S3† and Table 3). As seen from Table 3, the positive value of ΔH (16.49 kJ mol^{-1}) indicates that the adsorption of Cr(VI) was an endothermic reaction process. Moreover, it indicates that the adsorption was not a physical adsorption process because traditional physical adsorption is exothermic. For the positive value of ΔS°, it can demonstrate the enhanced randomness of the system, while the negative value of ΔG° confirms that the adsorption of Cr(VI) onto IIZMS-APTES was spontaneous.

3.3 Desorption and reusability study

The recycle ability of materials is a very important factor in industrial utility. In this study, the desorption of Cr(VI) ions from IIZMS-APTES was conducted with a 4 mol L^{-1} HNO$_3$

Table 2 Parameters of Langmuir and Freundlich models for Cr(VI) adsorption by IIZMS-APTES and NIZMS-APTES

Sample	Langmuir			Freundlich		
	q_m (mg g^{-1})	K_L (L mg^{-1})	R^2	K_F (mg g^{-1})	$1/n$	R^2
IIZMS-APTES	110.62	1.97×10^{-2}	0.9950	13.88	0.322	0.9593
NIZMS-APTES	74.35	1.21×10^{-2}	0.9937	6.95	0.355	0.9817

Table 4 K_d, K, K' parameters for IIZMS–APTES for competing adsorption

Competing adsorption		IIZMS-APTES			NIZMS-APTES			
		q_e (mg g^{-1})	K_d (L g^{-1})	K	q_e (mg g^{-1})	K_d (L g^{-1})	K	K'
Binary	Cr(VI)	51.52	1.00	532.45	12.34	0.14	9.19	57.94
	Cr(III)	0.17	1.88×10^{-3}		1.36	1.48×10^{-2}		
	Cr(VI)	47.37	0.92	264.00	7.86	8.66×10^{-2}	1.49	177.42
	Zn(II)	0.34	3.50×10^{-3}		5.36	5.82×10^{-2}		
	Cr(VI)	46.86	0.91	97.76	11.72	0.14	7.47	13.08
	Cu(II)	0.85	9.36×10^{-3}		1.64	1.82×10^{-2}		
Quaternary	Cr(VI)	51.29	1.289		4.86	5.64×10^{-2}		
	Cr(III)	0.71	6.86×10^{-3}	187.90	4.24	4.26×10^{-2}	1.32	141.98
	Zn(II)	0.37	3.78×10^{-3}	341.00	4.16	4.42×10^{-2}	1.28	267.24
	Cu(II)	4.56	0.047	27.19	4.00	3.97×10^{-2}	1.42	19.14

solution. The reusability was evaluated over five cycles of consecutive desorption–adsorption process (Fig. 7). It can be seen that the adsorption capacity of IIZMS-APTES still remained 53.37 mg g^{-1} after 5 cycles, and the removal efficiency is maintained above 90%. The result indicates that IIZMS-APTES has excellent regeneration property.

3.4 Adsorption selectivity

The adsorption selectivity of IIZMS-APTES towards Cr(VI) were investigated using 30 mg of the adsorbent with 30 mL of the solution containing 100 mg L^{-1} of Cr(VI) and coexisting ions at pH 3 and 30 °C for 60 min. The relative selectivity coefficient K' is an indicator to the selectivity performance for ion imprinting. It demonstrates significant adsorption selectivity while the value of K' is beyond 3.0.[23] The adsorption results and the selectivity parameters were listed in Table 4. It shows that the adsorption capacity of Cr(VI) on IIZMS-APTES is obviously higher than other ions, such as Cr(III), Cu(II), and Zn(II). It implies that the specific imprinted cavities on IIZMS-APTES particle play an important role in the adsorption of Cr(VI) when competing with other ions. It can be seen that in binary mixtures, the values of K' are 57.94, 13.08, and 177.42 for Cr(VI)/Cr(III), Cr(VI)/Cu(II), and Cr(VI)/Zn(II), respectively. Furthermore, in quaternary mixtures, the values of K' are 141.98 (Cr(III)), 267.24 (Zn(II)), and 19.14 (Cu(II)), respectively. All the values of K′ are much higher than 3, suggesting that IIZMS-APTES exhibits excellent adsorption selectivity towards Cr(VI) ions.

4. Conclusions

In this study, APTES functionalized molecular sieve 5A was used as the ion imprinting matrix. 4-VP was used as the ionic imprinting group and coated onto the matrix by radical-induced polymerization in combination with the *in situ* co-precipitation method. The as-prepared IIZMS-APTES was applied for the removal of Cr(VI) from aqueous solutions. IIZMS-APTES showed good adsorption capacity for Cr(VI) in acidic conditions. The adsorption processes followed the Langmuir model and the pseudo-second-order model. The thermodynamic study indicated that the adsorption process was endothermic and

spontaneous. Moreover, IIZMS-APTES showed excellent adsorption selectivity of Cr(VI) in solutions with co-existing ions.

Conflicts of interest

There are no conflicts to declare.

Acknowledgements

References

1 M. E. Mahmoud, *J. Environ. Manage.*, 2015, **147**, 264–270.
2 Y. Xu, J. Chen, R. Chen, P. Yu, S. Guo and X. Wang, *Water Res.*, 2019, **160**, 148–157.
3 R. M. Coyte, K. L. McKinley, S. Jiang, J. Karr, G. S. Dwyer, A. J. Keyworth, C. C. Davis, A. J. Kondash and A. Vengosh, *Sci. Total Environ.*, 2020, **711**, 135135.
4 T. Luo, X. Tian, C. Yang, W. Luo, Y. Nie and Y. Wang, *J. Agric. Food Chem.*, 2017, **65**, 7153–7158.
5 J. Ali, L. Wang, H. Waseem, R. Djellabi, N. A. Oladoja and G. Pan, *Chem. Eng. J.*, 2020, **384**, 123335.
6 A. Cimen, *Russ. J. Phys. Chem. A*, 2015, **89**, 1238–1243.
7 F. A. S. Moranchell, J. M. S. Pineda, J. N. H. Pérez, U. S. Silva-Rivera, C. A. C. Escobedo and R. D. G. G. Huerta, *Int. J. Hydrogen Energy*, 2020, **45**, 13683–13692.
8 D. Mahringer, S. S. Zerelli, U. Dippon and A. S. Ruhl, *Sep. Purif. Technol.*, 2020, **253**, 117478.
9 F. Sellami, O. Kebiche-Senhadji, S. Marais, L. Colasseand K. Fatyeyeva, *Sep. Purif. Technol.*, 2020, **248**, 117038.
10 S. Bao, W. Yang, Y. Wang, Y. Yu, Y. Sun and K. Li, *Chem. Eng. J.*, 2020, **399**, 125762.
11 J. Zhao, L. Yu, H. Ma, F. Zhou, K. Yang and G. Wu, *J. Colloid Interface Sci.*, 2020, **578**, 650–659.
12 E. T. Liu, H. Zhao, H. Li, G. Li, Y. Liu and R. Chen, *New J. Chem.*, 2014, **38**, 2911.
13 T. Sathish, N. V. Vinithkumar, G. Dharani and R. Kirubagaran, *Appl. Water Sci.*, 2014, **5**, 153–160.

14 M. Forghani, A. Azizi, M. J. Livani and L. A. Kafshgari, *J. Solid State Chem.*, 2020, **291**, 121636.

15 Q. Li, B. B. Guan, W. Zhu, T. H. Liu, L. H. Chen, Y. Wang and D. X. Xue, *J. Solid State Chem.*, 2020, **291**, 121672.

16 L. Rani, J. Kaushal, A. L. Srivastav and P. Mahajan, *Environ. Sci. Pollut. Res.*, 2020, 1–26.

17 G. Wulff, *Angew. Chem., Int. Ed.*, 1972, **11**, 341–346.

18 Z. Ren, D. Kong, K. Wang and W. Zhang, *J. Mater. Chem. A*, 2014, **2**, 17952–17961.

19 J. Zeng, J. Zeng, H. Zhou, G. Liu and Z. Y. J. Jian, *Front. Chem. Sci. Eng.*, 2020, **14**, 1–11.

20 T. Fang, X. Yang, L. Zhang and J. Gong, *J. Hazard. Mater.*, 2016, **312**, 106–113.

21 M. Taghizadeh and S. Hassanpour, *Polymer*, 2017, **132**, 1–11.

22 R. Huang, X. Ma, X. Li, L. Guo, X. Xie, M. Zhangand and J. Li, *J. Colloid Interface Sci.*, 2018, **514**, 544–553.

23 Y. A. B. Neolaka, G. Supriyanto, H. Darmokoesoemo and H. S. Kusuma, *J. Environ. Chem. Eng.*, 2018, **6**, 3436–3443.

24 E. Z. Piña-Salazar, T. Sakai, E. Ōsawa, R. Futamura and K. Kaneko, *J. Colloid Interface Sci.*, 2019, **549**, 133–139.

25 S. Godbout, V. R. Phillips and R. W. Sneath, *Biosyst. Eng.*, 2006, **95**, 1–6.

26 Z. Z. Mutasim and J. H. Bowen, *Chem. Eng. Res. Des.*, 1991, **69**, 108–118.

27 J. E. Romo, T. Wu, X. Huang, J. Lucero, J. L. Irwin, J. Q. Bond, M. A. Carreon and S. G. Wettstein, *ACS Omega*, 2018, **3**, 16253–16259.

28 Z. Yang, X. Chen, S. Li, W. Ma, Y. Li, Z. He and H. Hu, *Environ. Sci. Pollut. Res.*, 2020, **27**, 10899–10909.

29 P. Janik, B. Zawisza, E. Talik and R. Sitko, *Microchim. Acta*, 2018, **185**, 117.

30 N. Sana, B. Humaira, G. Abdul, T. Eylül, O. Zehra, D. Hatice and Y. Basit, *RSC Adv.*, 2018, **8**, 23963–23972.

31 M. Geszke-Moritz and M. Moritz, *Appl. Surf. Sci.*, 2016, **368**, 348–359.

32 N. Ozkantar, M. Soylak and M. Tuzen, *Atom. Spectros*, 2020, **41**, 43–50.

33 H. Vergara-Castaenda, A. R. Hernández-Martínez, M. Estévez, S. Mendoza, G. Luna-Barcenas and H. Pool, *J. Colloid Interface Sci.*, 2016, **466**, 44–55.

34 D. Kong, F. Zhang, K. Wang, Z. Renand and W. Zhang, *Ind. Eng. Chem. Res.*, 2014, **53**, 4434–4441.

35 N. Sun, Q. P. Zhang, H. R. Sun, W. B. Yang, Y. L. Zhou, J. F. Song and D. L. Luo, *Adv. Eng. Mater.*, 2018, **20**, 1700745.

36 M. M. J. Treacy, J. B. Higgins, *Collection of Simulated Xrd Powder Patterns for Zeolites*, 2007, vol. 10, pp. 26–27.

37 M. Maache, A. Janin, J. C. Lavalley and E. Benazzi, *Zeolites*, 1995, **15**, 507–516.

38 E. Khoramzadeh, M. Mofarahiand and C.-H. Lee, *J. Chem. Eng. Data*, 2019, **64**, 5648–5664.

39 L. Chen, Y. W. Wang, M. Y. He, Q. Chen and Z. H. Zhang, *Adsorption*, 2016, **22**, 309–314.

40 V. Pakade, E. Cukrowska, J. Darkwa, N. Torto and L. Chimuka, *Water SA*, 2011, **37**, 529–538.

41 O. B. Nchoe, M. J. Klink, F. M. MtunziandV and E. Pakade, *J. Mol. Liq.*, 2020, **298**, 111991.

42 A. Kara, E. Demirbel, N. Tekin, B. Osman and N. Besirli, *J. Hazard. Mater.*, 2015, **286**, 612–623.

43 D. D. Maksin, A. B. Nastasovic, A. D. Milutinovic-Nikolic, L. T. Surucic, Z. P. Sandic, R. V. Hercigonja and A. E. Onjia, *J. Hazard. Mater.*, 2012, **209–210**, 99–110.

44 M. Zhu, D. Fan, B. Liu, S. Liu and S. Tan, *J. Inorg. Mater.*, 2020, **35**, 309–314.

45 Q. Liang, J. Geng, H. Luo, W. Fang and Y. Yin, *J. Mol. Liq.*, 2017, **248**, 767–774.

46 S. Debnath and U. C. Ghosh, *J. Chem. Thermodyn.*, 2008, **40**, 67–77.